Supporting Information

Smith et al. 10.1073/pnas.1210126110

SI Materials and Methods

Additional Patient Characteristics. Because the present multivariate pattern analysis (MVPA) requires a high number of participants and only about 2% of patients with acute left hemisphere damage show full-blown spatial neglect (1), we thus restricted the present investigation to only those patients with a lesion of the right hemisphere. The sample of 140 patients, originally reported by Karnath et al. (2), used all stroke patients with circumscribed right hemisphere lesions consecutively admitted from a well-defined recruitment area belonging to the University of Tübingen over a period of 7 y. Three exclusion criteria were used: (*i*) patients with diffuse or bilateral brain lesions; (*ii*) patients with tumors; and (*iii*) patients in whom MRI or CT scans revealed no obvious lesion. We note that hemianopia was not an exclusion criterion. Patients were classified as neglect patients on fulfilling the criterion for spatial neglect in at least two of four traditional clinical tests for spatial neglect, namely the letter cancellation task (3), the Bells test (4), the baking tray task (5), and/or a copying task (6). All other patients were considered control patients. Notably, the resulting groups of neglect and control patients had comparable frequencies of visual field deficits (neglect patients: 23%; control patients: 29%; $\chi^2 = 0.67$, $P = 0.41$), indicating that the high classification accuracy of regions in visual cortex was not simply due to systematic differences in visual field deficits. Full demographic details can be found in table 1 of our original work (2).

Thus, although our findings may not generalize to rare cases of left hemisphere neglect patients (1, 7), we note that our results are generalizable to the vast majority of neglect patients—those with right hemisphere damage (for review, see refs. 8 and 9).

Imaging Procedures. Lesion location and extent was visualized using either MRI or CT. Lesion mapping was based on diffusion-weighted imaging (DWI) for MRI occurring within the first 48 h after stroke and T2-weighted fluid-attenuated inversion-recovery (FLAIR) sequences when MR imaging was conducted 48 h or later after the stroke. The mean time between lesion and the MRI was 5.0 d (SD = 5.4). In those subjects who underwent the CT imaging protocol, the mean time since lesion and the CT was 6.7 d (SD = 8.4). All lesions were marked manually (by an expert who was blind regarding the diagnosis of spatial neglect) on axial slices of a T1-weighted template MRI scan from the Montreal Neurological Institute (MNI) using the MRIcro software package (10) with a 1 × 1-mm in-plane resolution. This template is approximately oriented to match the Talairach coordinate system and is distributed with MRIcro. Lesions were mapped onto the slices that correspond to *Z*-coordinates (−40, −32, −24, −16, −8, 0, 8, 16, 24, 32, 40, and 50 mm) in MNI space by using the identical or the closest matching axial slices of each individual. The full details regarding imaging protocols and parameters are reported in our previous work, which used the same population of patients (2).

Combinatoric Analyses. These analyses involved our regions of interest (ROIs). We extended our ROI-based results by constructing combinations of two and three ROIs to be used as feature spaces. Adding this analysis to our 45 ROIs yielded 990 combinations of 2 ROIs and 14,190 combinations of 3 ROIs. Importantly, this approach allowed us to directly assess the contribution of the lesion size when explicitly included as a feature. Here, the emphasis switches to increases or decreases in cross-validation (CV) rather than absolute prediction levels.

The combinatoric approach can reveal two different traits for a given ROI (*i*) when combined with another ROI or set of ROIs (*j*). For example, in a combination of three (ROI A, ROI B, and ROI C), *j* would index all possible combinations of two (ROI A and ROI B) and how a single region (ROI C) improved on the predictive power of the combination of two (that did not include ROI C already). Therefore, *i* would index how any single region (ROI C) improved—on average—with the addition of any possible combination of two regions.

The specific metrics to consider are the following. First, consider that a given ROI (*i*) may consistently increase the predictive power (which we measure using CV) of a classifier when combined with other regions, indicating ROI (*i*) contains unique information. This trait—unique combinatorial performance (UCP)—has been used previously (11–13) and is defined in Eq. **S1**:

$$UCP_i \equiv \frac{\sum_{j=1}^{N} CV_{ij} - CV_j}{N}. \quad \textbf{[S1]}$$

In contrast, it may be the case that whenever ROI (*j*) is added to another ROI (*i*), the resulting predictive power of that classifier is improved, indicating that ROI (*i*) is missing information relevant to predicting the presence or absence of neglect. This trait—average combinatorial improvement (ACI)—has been used previously (11) and is defined in Eq. **S2**:

$$ACI_i \equiv \frac{\sum_{j=1}^{N} CV_{ij} - CV_i}{N}. \quad \textbf{[S2]}$$

Monte Carlo Permutation-Based Statistical Testing. Our hypothesis is that the MVPA of brain injury can accurately predict spatial neglect, whereas the null hypothesis is that we cannot reliably distinguish this disorder. Our aim was to validate whether our classification significantly outperforms chance performance. To evaluate these tests, we used Monte Carlo permutation-based statistical testing, where each of our analyses was permuted 1,000 times with randomized labels for neglect and control patients (14). This process allowed us to construct null distributions that were used to examine whether a given CV percentage (or change in CV percentage) was significant at an α of $P = 0.05$ (i.e., test value >95th percentile for a one-tailed test; test value <2.5 percentile or test value >97.5 percentile for a two-tailed test). Except where noted, we emphasize that permutation-based testing afforded us an opportunity to control for multiple comparisons in our ROI-based analyses, where hundreds of separate (but nonindependent) analyses were conducted (14).

Similar methods were used for statistical inference on our combinatoric analyses. These analyses quantify two pieces of information regarding the interplay between a given ROI (or feature) and other ROIs. First, we can examine how a specific ROI changes the predictive power, on average, of other ROIs when added to those ROIs (Eq. **S1**). Second, we can examine how a particular ROI's predictive power changes, on average, when other ROIs are added to it (Eq. **S2**). This method provides a mechanism to both assess if a particular ROI is consistently able to improve predictions, and if an ROI can consistently be missing predictive information. To assess the statistical significance of these two types of changes, we computed, for each ROI, a one-sample *t* test against a null hypothesis of an average CV change of zero; the resulting *P* values were then Bonferroni corrected for multiple comparisons.

SI Results

In addition to our primary analyses on ROIs, we examined several additional multivariate feature spaces. We also performed numerous control analyses to quantify and control for the effects of lesion size.

Additional Multivariate Feature Spaces. ***Two-dimensional feature spaces.*** Given the importance of the lesion size, we first repeated all single voxel classifications with lesion size included as its own feature, forming a 2D (i.e., multivariate) feature space for each classification. Importantly, voxels in the superior temporal gyrus (STG) were least affected by the inclusion of lesion size information, suggesting that lesion size does not provide independent information when combined with the STG and adjacent perisylvian regions (Fig. S1*B*). In contrast, we also found several voxels whose performance improved as a result of including of lesion size information, with a peak voxel falling within visual cortex ($MNI_{(x,y,z)}$ = 14,−96,−10; CV = 82.28%, P_{perm} < 0.0001).

We next examined whether the best-performing voxel in this analysis—a single voxel within visual cortex with lesion size included as its own feature (CV = 82.28%)—outperformed the two best univariate predictors: lesion size (CV = 78.14%) and a voxel within STG (CV = 73.57%). Although our analysis indicated that the gain over the lesion size was only trending toward significance ($CV_{increase}$ = 4.14, P_{perm} = 0.0779), the gain over the best-performing voxel in STG was significant ($CV_{increase}$ = 8.71, P_{perm} < 0.0001), indicating a substantial increase in predictive power with the addition of a single piece of information.

Whole-brain feature spaces. As single voxels are unlikely to carry maximal predictive power for spatial neglect—even when including additional information such as lesion size—our next analyses examined multiple voxels across the whole brain simultaneously. We conducted this analysis with and without the lesion size feature included in the model. We also compared these results across two types of masks, which either included any voxel damaged across the 140 patients or included only voxels damaged in at least 5% of patients (Fig. 1*B*). Across all of these tests, the CVs were significantly above chance, ranging from 81.71% to 83.00% (permutation tests, all P < 0.00001). We did not observe any differences between these tests (permutation tests, all P > 0.45).

We additionally tested whether these whole-brain classifications were better than our two best univariate predictors: lesion size and a single voxel with STG. We found that all four whole-brain CVs were significantly higher than the voxel within STG (CV increases: 9.14, 9.00, 8.42, 9.42; all P < 0.001). In a parallel comparison against lesion size, we failed to find evidence for a significant gain in performance with the addition of other voxels throughout the brain (all CV increases < 4.85; all P > 0.189).

Perisylvian ROIs with lesion size included as its own feature. For a baseline comparison, we examined the results of each ROI analysis performed independently and with lesion size included as its own feature (Fig. S2). After adding lesion size as a feature, several classifiers trained on particular regions improved performance, although this gain was significant only in the inferior frontal gyrus pars orbitalis. Inclusion of lesion size reduced performance for both the supramarginal gyrus and insula, but neither decrease was statistically significant.

Controlling for Lesion Size. ***Adjusting cross-validation rates using a regression model.*** We reasoned that the performance of each ROI (or ROI combination) could be influenced by the overall size of a given ROI/combination and the difference in average damage (within that ROI/combination) between neglect and control patients. Consistent with a prior fMRI study controlling for ROI size (12), we computed size- and lesion-adjusted CVs. These adjustments were made using a regression model including ROI size and difference in lesion damage between groups (Table S4). After estimating the linear effect of ROI size on CV percentage, we computed, for each permutation, the predicted performance of each ROI and then subtracted that from the observed performance. Thus, this procedure effectively regresses out the contribution of between-group lesion size disparity and ROI size.

Using these adjusted CV percentages, we examined the robustness of our claim regarding the gain in performance when adding brain regions to a classifier. We first compared the average CV percentages of all single ROIs, combinations of two ROIs, and combinations of three ROIs (Fig. S3*A*). As the underlying distribution corresponding to changes in average adjusted CV percentage is unknown, we constructed null distributions using Monte Carlo permutation-based testing (see histograms in Fig. S3 *B* and *C*), which entailed running all analyses 1,000 times with permuted neglect and control labels. For each permutation, we computed the change in average adjusted CV percentage for both comparisons (i.e., 2 ROIs – 1 ROI; and 3 ROIs – 2 ROIs). Our results showed that the average adjusted CV for combinations of two ROIs was significantly higher compared with single ROIs ($CV_{increase}$ = 8.9, P < 0.001; Fig. S3*B*). Additionally, we found that the average adjusted CV percentage was significantly higher for combinations of three ROIs compared with combinations of two ROIs ($CV_{increase}$ = 4.9, P < 0.005; Fig. S3*C*).

Nonindependence across features. Larger lesions could be associated with correlated patterns of damage in specific areas, producing nonindependence across features. We note that the issue of nonindependence—i.e., spatial correlation—does not generally affect performance measures for the support vector machine (SVM) classifiers used in our work (15–17). Nonindependence would, however, affect the feature weights in a given classification. Specifically, in a linear SVM, feature weights on correlated features (i.e., regions that are affected together) would be shrunk proportionally to the number of correlated voxels (18). Furthermore, we note that SVMs do not have assumptions regarding independence between features (unlike, for example, a naïve Bayes classifier). Indeed, nearly all MVPA studies—particularly those using searchlights—have highly correlated features (11, 19, 20). Thus, even though there is some correlation between our features (Fig. S4*A*; mean: 0.16) and a scant amount of redundancy (Fig. S4*B*; mean: 0.005%), classifiers constructed using SVM algorithms should be expected to work well with lesion data. Importantly, we also note that the majority of our features (67%) were unique, and all ROIs were able to contribute unique features (range: 11–100%) to each classification. Within the 12 perisylvian regions, we observed similar proportions of unique features (mean: 67%; range: 23–84%).

1. Becker E, Karnath HO (2007) Incidence of visual extinction after left versus right hemisphere stroke. *Stroke* 38(12):3172–3174.
2. Karnath H-O, Fruhmann Berger M, Küker W, Rorden C (2004) The anatomy of spatial neglect based on voxelwise statistical analysis: A study of 140 patients. *Cereb Cortex* 14(10):1164–1172.
3. Weintraub S, Mesulam M (1985) Mental state assessment of young and elderly adults in behavioral neurology. *Principles of Behavioral Neurology*, ed Mesulam M (Davis Company, Philadelphia), pp 71–123.
4. Gauthier L, Dehaut F, Joanette Y (1989) The Bells test: A quantitative and qualitative test for visual neglect. *Int J Clin Neuropsychol* 11(2):49–54.
5. Tham K, Tegner R (1996) The baking tray task: A test of spatial neglect. *Neuropsychol Rehabil* 6(1):19–26.
6. Johannsen L, Karnath HO (2004) How efficient is a simple copying task to diagnose spatial neglect in its chronic phase? *J Clin Exp Neuropsychol* 26(2):251–256.
7. Suchan J, Karnath HO (2011) Spatial orienting by left hemisphere language areas: A relict from the past? *Brain* 134(Pt 10):3059–3070.
8. Karnath HO, Rorden C (2012) The anatomy of spatial neglect. *Neuropsychologia* 50(6): 1010–1017.
9. Corbetta M, Shulman GL (2011) Spatial neglect and attention networks. *Annu Rev Neurosci* 34(1):569–599.

10. Rorden C, Brett M (2000) Stereotaxic display of brain lesions. *Behav Neurol* 12(4): 191–200.
11. Clithero JA, Carter RM, Huettel SA (2009) Local pattern classification differentiates processes of economic valuation. *Neuroimage* 45(4):1329–1338.
12. Carter RM, Bowling DL, Reeck C, Huettel SA (2012) A distinct role of the temporal-parietal junction in predicting socially guided decisions. *Science* 337(6090):109–111.
13. Hampton AN, O'doherty JP (2007) Decoding the neural substrates of reward-related decision making with functional MRI. *Proc Natl Acad Sci USA* 104(4):1377–1382.
14. Nichols TE, Holmes AP (2002) Nonparametric permutation tests for functional neuroimaging: A primer with examples. *Hum Brain Mapp* 15(1):1–25.
15. Hastie T, Tibshirani R, Friedman J (2009) *The Elements of Statistical Learning* (Springer, New York).
16. Schölkopf B, Smola AJ (2001) *Learning with Kernels: Support Vector Machines, Regularization, Optimization, and Beyond* (MIT Press, Cambridge, MA).
17. Mourão-Miranda J, Bokde AL, Born C, Hampel H, Stetter M (2005) Classifying brain states and determining the discriminating activation patterns: Support vector machine on functional MRI data. *Neuroimage* 28(4):980–995.
18. Pereira F, Mitchell T, Botvinick M (2009) Machine learning classifiers and fMRI: A tutorial overview. *Neuroimage* 45(1 Suppl):S199–S209.
19. Kriegeskorte N, Goebel R, Bandettini P (2006) Information-based functional brain mapping. *Proc Natl Acad Sci USA* 103(10):3863–3868.
20. Clithero JA, Smith DV, Carter RM, Huettel SA (2011) Within- and cross-participant classifiers reveal different neural coding of information. *Neuroimage* 56(2):699–708.
21. Tzourio-Mazoyer N, et al. (2002) Automated anatomical labeling of activations in SPM using a macroscopic anatomical parcellation of the MNI MRI single-subject brain. *Neuroimage* 15(1):273–289.
22. Bürgel U, et al. (2006) White matter fiber tracts of the human brain: three-dimensional mapping at microscopic resolution, topography and intersubject variability. *Neuroimage* 29(4):1092–1105.

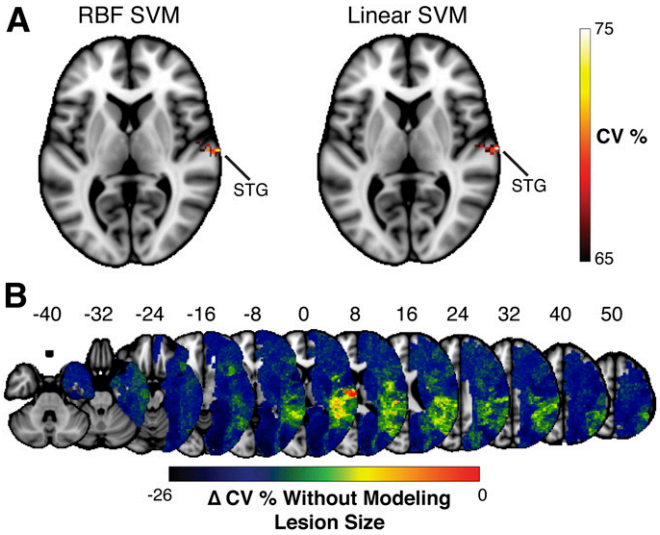

Fig. S1. Performance of individual voxels in predicting neglect. (*A*) Using both linear and nonlinear [radial basis function kernel (RBF)] SVM classifiers, we found that voxels within the STG were significantly above chance performance (maximum CV = 75.00%, $P < 0.05$, Bonferroni correction across all voxels). To reveal the spatial extent of these findings, the maps are thresholded at $P < 0.001$ uncorrected (axial slice at $Z = 0$ in MNI space). (*B*) We additionally examined how each voxel changed when modeling lesion size explicitly as its own feature. We found several voxels within visual frontal cortices whose performance was worse without lesion size modeled as its own feature. Importantly, perisylvian regions, including the STG, were least affected by the inclusion of lesion size, indicating that the predictive power within these regions is not enhanced by lesion size. Axial slice numbers are provided in terms of MNI space.

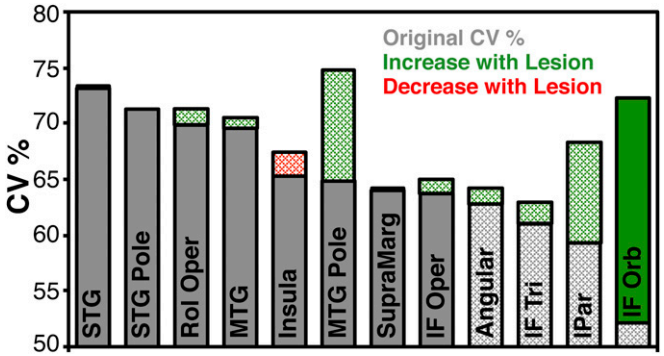

Fig. S2. Effects of including lesion size as a feature in single ROI classifications. For a baseline comparison, we also show the results of each ROI analysis performed independently and with lesion size included as its own feature. The STG was the strongest predictor of neglect before adding the lesion size feature (gray bars; solid color denotes statistical significance at $P < 0.05$ corrected). After including lesion size as its own feature, several regions improved performance, although this gain was significant only in the inferior frontal gyrus pars orbitalis (IF Orb; green bars; solid color denotes statistical significance at $P < 0.05$ corrected). Inclusion of lesion size reduced performance for both the supramarginal gyrus and insula (red bars), but neither decrease was statistically significant.

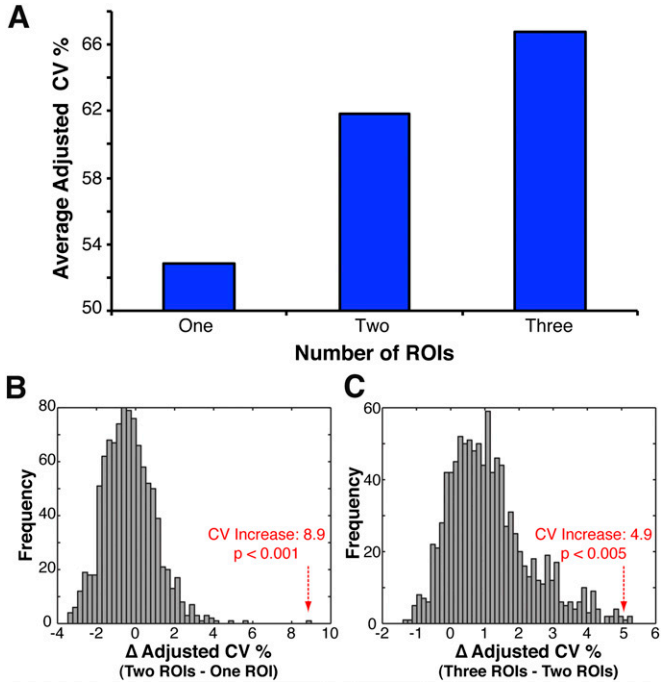

Fig. S3. Additional brain regions improve predictive power. (*A*) Modeling multiple brain regions is a key advance of our multivariate lesion-mapping approach; however, this benefit could be explained by ROI size and/or lesion size. We therefore computed ROI size– and lesion size–adjusted CVs based on a regression model (Table S4). Here we show the average adjusted CV percentages across all single ROIs ($n = 45$), all combinations of two ROIs ($n = 990$), and all combinations of three ROIs ($n = 14{,}190$). As the underlying distribution corresponding to changes in average adjusted CV percentage is unknown, we constructed null distributions (histograms shown) by running all analyses 1,000 times with permuted neglect and control labels. For each permutation, we computed the change in average adjusted CV percentage for both comparisons (i.e., 2 ROIs – 1 ROI; and 3 ROIs – 2 ROIs). (*B*) We found that the average adjusted CV increased when adding one ROI to another ROI ($CV_{increase} = 8.9$, $P < 0.001$; red line). (*C*) Additionally, we found that the average adjusted CV increased when adding one ROI to two ROIs ($CV_{increase} = 4.9$, $P < 0.005$; red line). Data in histograms are partitioned into 50 equally spaced bins on the *x*-axis.

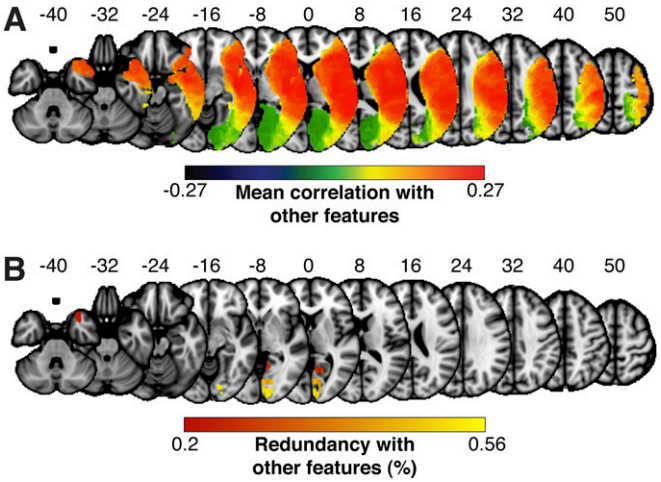

Fig. S4. Feature correlations. (*A*) On average, we found that most features exhibited a small degree of correlation with other features. This finding highlights the importance of using classifiers that do not assume independence between features. (*B*) We also examined whether any features were redundant with other features. Although we found an exceedingly small amount of redundancy across our features, we note that these heavily redundant features were outside of perisylvian regions. For clarity, the redundancy map here was thresholded using the 95th percentile of the distribution of feature redundancy. The numerical range shown on the map is therefore 0.002 (0.2%) to 0.0056 (0.56%), which translates to 26–72 features.

Table S1. ROIs

Name	Size (full mask)	Size (restricted mask)	Tissue type
Precentral	481	434	GM
Frontal_Sup	588	14	GM
Frontal_Sup_Orb	105	*	GM
Frontal_Mid	911	442	GM
Frontal_Mid_Orb	169	49	GM
Frontal_Inf_Oper	**360**	**354**	**GM**
Frontal_Inf_Tri	**506**	**496**	**GM**
Frontal_Inf_Orb	**348**	**267**	**GM**
Rolandic_Oper	**347**	**347**	**GM**
Supp_Motor_Area	196	*	GM
Olfactory	14	3	GM
Frontal_Sup_Medial	270	*	GM
Frontal_Mid_Orb	195	*	GM
Rectus	74	*	GM
Insula	**485**	**484**	**GM**
Cingulum_Ant	245	*	GM
Cingulum_Mid	320	*	GM
Cingulum_Post	18	*	GM
Hippocampus	198	39	GM
ParaHippocampal	224	9	GM
Amygdala	55	41	GM
Calcarine	431	414	GM
Cuneus	314	138	GM
Lingual	626	432	GM
Occipital_Sup	301	172	GM
Occipital_Mid	486	460	GM
Occipital_Inf	247	224	GM
Fusiform	562	117	GM
Postcentral	566	554	GM
Parietal_Sup	311	161	GM
Parietal_Inf	**261**	**246**	**GM**
SupraMarginal	**338**	**338**	**GM**
Angular	**370**	**363**	**GM**
Precuneus	488	39	GM
Paracentral_Lobule	68	*	GM
Caudate	228	171	GM
Putamen	266	238	GM
Pallidum	70	63	GM
Thalamus	184	26	GM
Heschl	92	92	GM
Temporal_Sup	**818**	**818**	**GM**
Temporal_Pole_Sup	**281**	**224**	**GM**
Temporal_Mid	**1,061**	**1,061**	**GM**
Temporal_Pole_Mid	**313**	**197**	**GM**
Temporal_Inf	790	399	GM
Acoustic_radiation	7	7	WM
Callosal_Body	662	333	WM
Cingulum	3	*	WM
Corticospinal_tract	363	330	WM
Fornix	2	*	WM
Inferior_occipito-frontal_fascicle	43	43	WM
Optic_radiation	416	402	WM
Superior_longitudinal_fascicle	55	55	WM
Superior_occipito-frontal_fascicle	13	13	WM
Uncinate_fascicle	9	9	WM
semiovale_WM	605	384	WM

From the Automated Anatomical Labeling (AAL) and Juelich atlases, we identified 56 ROIs to use in our classifications. The number of voxels in each ROI is presented for both the full mask (i.e., union of all lesions) and the restricted mask (i.e., damaged in at least 5% of patients). Regions in bold (n = 12) represent critical perisylvian regions that have previously been associated with spatial neglect in the literature. Ant, anterior; GM, gray matter; Inf, inferior; Mid, middle; Oper, operculum; Orb, orbital; Post, posterior; Sup, superior; Tri, triangularis; WM, white matter; *, regions that did not exist after restricting the mask.

Table S2. Single ROIs performing significantly above chance

ROI	CV%	Corrected *P* value
Corticospinal_tract	75.85	<0.0001
Semiovale_WM	75.14	<0.0001
Temporal_Sup	73.14	<0.0001
Heschl	72.00	<0.0001
Temporal_Pole_Sup	71.28	<0.0001
Postcentral	70.71	<0.0001
Superior_longitudinal_fascicle	70.57	<0.0001
Rolandic_Oper	69.85	<0.0001
Temporal_Mid	69.57	<0.0001
Inferior_occipito-frontal_fascicle	68.00	<0.001
Optic_radiation	68.00	<0.001
Callosal_Body	67.57	<0.001
Insula	67.42	<0.001
Precentral	67.28	<0.01
Putamen	66.57	<0.01
Temporal_Pole_Mid	64.85	<0.05
Caudate	64.71	<0.05
SupraMarginal	64.14	<0.05
Frontal_Inf_Oper	63.71	<0.05
Superior_occipito-frontal_fascicle	63.42	<0.05

We found several regions whose CV rates were significantly above chance, even after correcting for multiple comparisons across all 45 regions of interest. Gray matter terminology follows the AAL atlas. White matter terminology follows Juelich atlas. Brain matter not contained in either atlas is identified as semiovale white matter (semiovale_WM). Ant, anterior; Inf, inferior; Mid, middle; Oper, operculum; Orb, orbital; Post, posterior; Sup, superior; Tri, triangularis.

Table S3. Single ROIs whose performance changes when including lesion size as its own feature

ROI	CV%: ROI	CV%: ROI + lesion size feature	Increase in CV%	Corrected *P* value
Frontal_Mid_Orb	45.14	76.14	31.00	<0.01
Calcarine	50.00	78.71	28.71	<0.01
Lingual	51.00	78.57	27.57	<0.01
ParaHippocampal	52.71	79.57	26.85	<0.01
Occipital_Inf	50.85	76.28	25.42	<0.01
Thalamus	55.28	79.42	24.14	<0.01
Parietal_Sup	54.42	78.28	23.85	<0.01
Frontal_Mid	54.14	77.42	23.28	<0.05
Olfactory	55.71	79.00	23.28	<0.05
Cuneus	56.00	78.85	22.85	<0.05
Occipital_Sup	56.28	78.85	22.57	<0.05
Precuneus	52.85	75.14	22.28	<0.05
Uncinate_fascicle	56.00	77.14	21.14	<0.05
Frontal_Sup	55.57	76.57	21.00	<0.05
Fusiform	57.71	78.00	20.28	<0.05
Frontal_Inf_Orb	52.14	72.28	20.14	<0.05

We identified several ROIs whose performance changed significantly when including lesion size as its own feature. These results therefore highlight regions that depend on information regarding lesion size. Gray matter terminology follows the AAL atlas (1). White matter terminology follows Juelich atlas (2). Brain matter not contained in either atlas is identified as semiovale white matter (semiovale_WM). Ant, anterior; Inf, inferior; Mid, middle; Oper, operculum; Orb, orbital; Post, posterior; Sup, superior; Tri, triangularis.

1. Tzourio-Mazoyer N, et al. (2002) Automated anatomical labeling of activations in SPM using a macroscopic anatomical parcellation of the MNI MRI single-subject brain. *Neuroimage* 15(1):273–289.
2. Bürgel U, et al. (2006) White matter fiber tracts of the human brain: three-dimensional mapping at microscopic resolution, topography and intersubject variability. *Neuroimage* 29(4): 1092–1105.

Table S4. Effects of ROI size and lesion size

ROI set	Lesion size effect	ROI size effect	Constant	Adjusted R^2
Without including lesion size as its own feature				
Single ROI	$\beta = 0.0101$	$\beta = 77.66$	52.83	0.34
	$t_{(42)} = 2.43$, $P < 0.05$	$t_{(42)} = 3.78$, $P < 0.01$		
Two ROIs	$\beta = 0.0052$	$\beta = 46.91$	61.83	0.19
	$t_{(987)} = 9.13$, $P < 0.001$	$t_{(987)} = 10.54$, $P < 0.001$		
Three ROIs	$\beta = 0.0032$	$\beta = 26.81$	66.77	0.12
	$t_{(14,987)} = 31.743$, $P < 0.001$	$t_{(14,987)} = 25.04$, $P < 0.001$		
With including lesion size as its own feature				
Single ROI	$\beta = -0.0096$	$\beta = -12.06$	76.83	0.21*
	$t_{(43)} = -3.34$, $P < 0.01$	$t_{(43)} = -0.86$, NS		
Two ROIs	$\beta = -0.0023$	$\beta = 13.52$	71.74	0.04*
	$t_{(1,032)} = -5.59$, $P < 0.001$	$t_{(1,032)} = 4.22$, $P < 0.001$		
Three ROIs	$\beta = 0.0011$	$\beta = 18.71$	69.93	0.05*
	$t_{(15,177)} = 13.86$, $P < 0.001$	$t_{(15,177)} = 21.91$, $P < 0.001$		

In our ROI-based analyses, we examined the relationship between performance (CV%) of each ROI (or ROI combination) and two variables: ROI size and absolute difference lesion size (i.e., proportion of ROI or ROI combination damaged) between neglect and control patients. Before including lesion size as its own feature, we observed, for each ROI set, a strong positive relationship between ROI performance and both lesion and ROI size. Specifically, as ROI size and the disparity in ROI damage between neglect and control patients increased, CV% increased. Using these estimates, we regressed out the influence of ROI size and lesion size for each ROI set where lesion size was not modeled as its own feature. Notably, a parallel relationship was not observed in the ROI sets where lesion size was included as its own feature, suggesting that the inclusion of lesion size as a feature partially accounts for its influence on ROI performance. Consistent with this idea, we also note that the adjusted R^2 for each of these regressions was significantly lower (*$P_{perm} < 0.001$) than the regressions where lesion size was not included as its own feature. NS, not significant.